



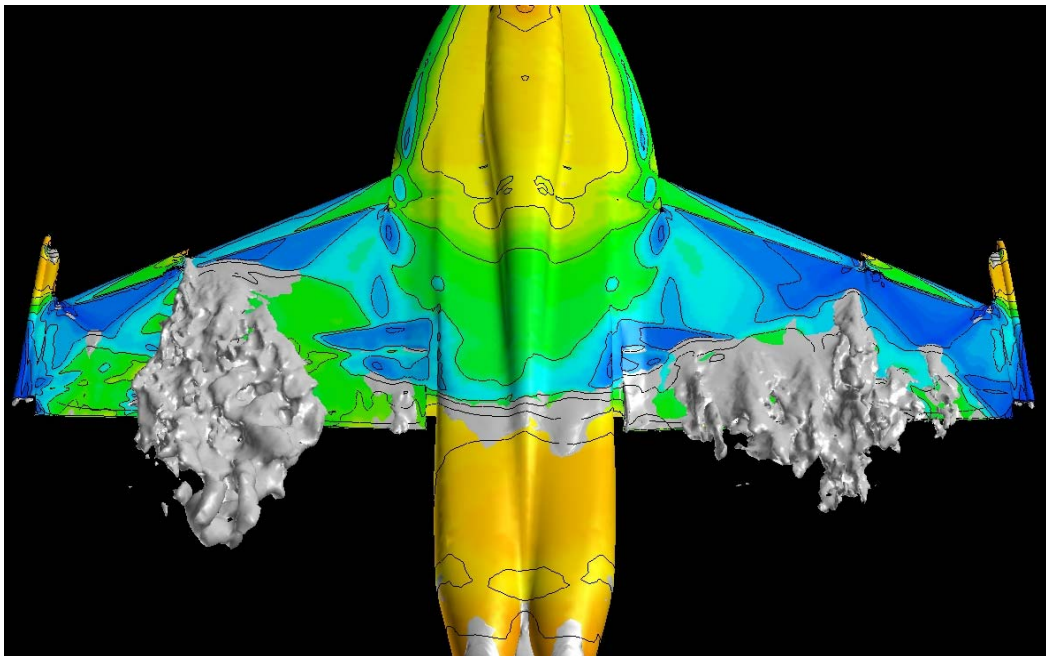
AIAA 2003-0592

**UNDERSTANDING ABRUPT WING STALL
WITH CFD**

S.H. Woodson, B.E. Green, J.J. Chung, D.V. Grove
Naval Air Systems Command, Patuxent River, MD

P.C. Parikh
NASA Langley Research Center, Hampton, VA

J.R. Forsythe
United States Air Force Academy, Colorado Springs, CO



**41st AIAA Aerospace Sciences Meeting & Exhibit
6-9 January 2003
Reno, Nevada**

For permission to copy or to republish, contact the copyright owner named on the first page.
For AIAA-held copyright, write to AIAA Permissions Department,
1801 Alexander Bell Drive, Suite 500, Reston, VA, 20191-4344

Understanding Abrupt Wing Stall with CFD

S.H. Woodson*, B.E. Green[†], J.J. Chung[†], D.V. Grove[†]
 Naval Air Systems Command
 Patuxent River, MD

P.C. Parikh*
 NASA Langley Research Center
 Hampton, VA

J.R. Forsythe[‡]
 United States Air Force Academy
 Colorado Springs, CO

Abstract

This paper describes the Computational Fluid Dynamics (CFD) efforts and lessons learned during the four-year Abrupt Wing Stall national research program. The paper details the complex nature of the transonic flows encountered by modern U.S. fighter and attack aircraft during transonic maneuvering conditions. Topics include grid resolution, computational memory and CPU requirements, turbulence modeling, steady and unsteady calculations, and Reynolds-Averaged-Navier-Stokes solutions compared with Detached Eddy Simulations for this highly complex, viscously-dominated, shock-induced, massively-separated class of flow.

Examples include results obtained for F/A-18C, AV-8B, pre-production F/A-18E, and F-16N aircraft undergoing transonic maneuvering conditions. Various flap settings have been modeled and the CFD results compared with extensive wind tunnel data. The comparisons illustrate the results obtained from both structured and unstructured CFD codes. The utility and accuracy of the various computational solvers is evaluated by qualitative comparisons of surface oil flow and pressure sensitive paint results obtained in wind tunnels for some of the models as well as by detailed quantitative pressure coefficient data where experimental results exist. Static lift coefficients are compared between CFD codes as well as the experimental data for each of the aircraft considered in this study.

Introduction

The Abrupt Wing Stall (AWS) Program was formed in response to a recommendation from a Department of Defense (DoD) commissioned blue ribbon panel, which called for a national research effort to investigate the fundamental causes of AWS.¹ The AWS Program is a joint NASA/Navy/Air Force applied research program with collaboration from universities and industry with the goals of: (1) providing a better understanding of the root causes of AWS, (2) develop figures-of-merit (FOM) for the

identification and characterization of AWS, and (3) develop computational, experimental, and simulation procedures and techniques that can be employed by future aircraft designers to recognize and eliminate unwanted lateral motions early in the design phase of a development program. This paper describes the results obtained from the computational efforts to meet the goal of providing a better understanding of AWS.

Background

Since the advent of fighter aircraft that can operate at transonic speeds and angles of attack (AoA) beyond which the airflow remains attached to the wings, there have been numerous examples of aircraft experiencing uncommanded lateral activity.² This type of motion has been variously characterized as

* Aerospace Engineer, Associate Fellow AIAA

† Aerospace Engineer, Senior Member AIAA

‡ Associate Professor, Senior Member AIAA

This paper is declared a work of the U.S. Government and is not subject to copyright protection in the United States.

“heavy wing”, “wing rock”, and “wing drop,” depending on the particular manifestation in each aircraft. The most recent encounter of the wing drop phenomenon was experienced during the Engineering & Manufacturing Development phase of the Navy F/A-18E/F program. At transonic Mach numbers, the airplane initially exhibited abrupt roll-offs of 40-60 degrees, passing through 8-10 degrees AoA. Though clearly unsatisfactory for mission purposes, this characteristic also precluded performance of many other types of testing. This led to a concentrated effort by the Navy and its contractors to identify the aerodynamic cause of this undesirable characteristic and to determine a low-cost, low-impact remedy.

Immediate dramatic improvement was achieved by a modification of the aircraft control laws to provide a more aggressive flap schedule in the relevant flight regime, thereby permitting other test disciplines to advance. The final production solution incorporated a porous fairing over the wing-fold mechanism. Those minor alterations were sufficient to suppress any adverse rolling moment encountered on the F/A-18E/F, but did little to provide a fundamental understanding of the flow physics causing the wing drop phenomenon.

CFD Codes Employed

Several computational approaches have been applied to the goal of providing a better understanding of the AWS phenomena, from panel codes, to steady state Euler and Reynolds-Averaged-Navier-Stokes (RANS) methods, to unsteady Detached Eddy Simulation (DES) Navier-Stokes solutions. After a brief description of three of the CFD codes employed by the AWS Program members, selected results from the application of those codes to the better understanding of AWS is presented.

USM3D

*USM3D*³ is a three dimensional, tetrahedral, cell-centered, finite-volume, Euler and Navier-Stokes flow solver for unstructured meshes. The inviscid flux quantities are computed across each cell face using Roe’s flux difference splitting. Spatial discretization is accomplished by a novel reconstruction process, which is based on an analytical formulation for computing solution gradients within tetrahedral cells. The solution is advanced to a steady state condition by an implicit backward-Euler time-stepping scheme. Flow turbulence effects are modeled by the Spalart-Allmaras (SA)⁴ one-equation model.

USM3D runs on massively parallel computers and on clusters of personal computers. Although a single processor version is available for a variety of computing platforms, the parallel version⁵ is the code of choice because it enables rapid turn-around for large problems.

WIND

The *WIND* flow solver⁶ is an extension of the *NASTD* chimera code, which was developed by McDonnell Douglas Aerospace-East. *WIND* solves the continuity, momentum, and energy equations in conservative form using second-order-accurate finite differences on structured, multi-zonal computational grids. The explicit terms are computed using either upwind or central differences. The implicit terms are computed using either an approximately factored or four-stage Runge-Kutta scheme. Several turbulence models are available within *WIND*. Menter’s Shear Stress Transport (SST) model⁷ was used during this research, since it was determined early in the AWS program that the solutions with *WIND* on the pre-production F/A-18E using SST correlated better with wind-tunnel results than did the results using the SA option.⁸

Cobalt

*Cobalt*⁹ is a cell-centered finite volume Navier-Stokes solver applicable to arbitrary cell topologies. The spatial operator uses the exact Riemann solver of Gottlieb and Groth¹⁰ allowing CFL numbers on the order of one million. It employs a least squares gradient calculation using QR factorization to provide second order accuracy in space and TVD flux limiters to limit extremes at cell faces. A point implicit method using analytic first-order inviscid and viscous Jacobians is used for advancement of the discretized system. For time accurate computations, a Newton sub-iteration scheme is employed, and the method is second order accurate in time.

Results

Aircraft Considered in the AWS Study

Four fighter and attack aircraft were considered during the CFD efforts of the AWS Program. Two were chosen because they are susceptible to AWS (the pre-production F/A-18E and the AV-8B outside its normal operating envelope) and two are not (the F/A-18C and the F-16N on flap schedule). They were also chosen because of wind tunnel model availability and the existence of transonic databases with which to validate the CFD results. Selected

geometric parameters of the aircraft are presented in Figure 1. As can be seen, each of the aircraft have moderate leading edge sweep angles and aspect ratios, but quite significant differences in thickness, twist, and dihedral (as well as airfoil sections). Another consideration of choosing these four aircraft was the intent to provide a large enough database so that reliable computational (and experimental¹¹) FOM could be developed for predicting the onset of an AWS event and a means of isolating the span-wise location and extent of the problem.

In addition to the aircraft listed in Figure 1, a F/A-18 “C to E wing morphing” study was undertaken,¹² in which each of the wing design changes that were incorporated for the F/A-18E that differed from the F/A-18C were varied in isolation and in limited combinations. The intent was to try and determine which of the wing design parameters were the major contributors to the AWS events experienced by pre-production F/A-18E/F aircraft. This was accomplished by beginning with the baseline F/A-18C and then modifying the geometry in the same manner as that which was incorporated for the F/A-18E wing design. Figure 2 provides a list of the major wing design differences between the F/A-18C and F/A-18E aircraft.

Lower Order Methods vs. RANS Analysis

During preliminary design of a new air vehicle, various design parameters are “traded” in an effort to meet mission and manufacturing requirements. At this stage, it is impracticable to perform a viscous, compressible analysis. However, a designer would like to know as early as possible if the proposed design may be susceptible to AWS. The question arises: Is there a quick and easy way to determine if my design will be subject to AWS? In an effort to answer that question we compare the results for the pre-production F/A-18E with flap deflections of 10/10/5 (leading edge [LE]/trailing edge [TE]/down aileron) obtained from a panel code with an inviscid, and a viscous *USM3D* calculation at 0.8 Mach number. Figure 3 illustrates the span-wise lift distribution determined from each method for various AoA.

In Figure 3a, the panel code predicts a continuous increase in overall lift as AoA is increased, as expected. Note that the reduction of lift at about 70% semi-span indicates that the reduction in camber due to the difference in the deflection angles of the TE flap and the aileron overcome the increase in lift due to the increased chord of the LE snag. Also obvious is the fact that maximum local lift is achieved

outboard of 50% semi-span and as the lift increases the center of lift moves outboard. This is of course a good indication of where along the span the wing will stall first (as can be seen from Figure 3c) and if that location is forward of the aileron, roll control may be diminished. Next consider the results from the Euler analysis. Here again, since the airflow is by definition attached, as AoA increases, overall lift increases and the center of lift moves outboard until a maximum is achieved at the highest AoA. Here, however, since the Euler solution is a field method, flow rotation caused by the tip vortex is successfully captured and the increased lift outboard is apparent compared to the panel method. Lastly, compare the results obtained from the viscous RANS calculation. Now overall lift is reduced because the flow separates forward of the TE even at the lowest AoA, and as AoA is increased, overall lift increases until between 7 and 8 degrees, where a significant reduction in lift is produced due to the flow separation reaching the LE as illustrated in Figure 4.

Figure 4 shows the upper surface pressure coefficient distribution over the wing of the pre-production F/A-18E, flaps 10/10/5 at 0.8 Mach for two AoA using the *USM3D* code with the SA turbulence option. The wing surface is color coded, with high-speed flow shown in red and lower speed flow indicated by yellow/green. At 7 degrees, there exists a jagged normal shock wave just aft of the LE flap hinge line in the region of the LE snag, which produces a flow separation, while at 8 degrees, the separation has jumped to the LE in the snag region and the subsequent loss of lift is produced. Figure 5 presents a comparison of the lift curves obtained with the Euler and RANS analysis. The inviscid result produces a linear lift curve and completely misses the break in the lift curve slope at 8 degrees AoA, which the viscous result accurately captures. A change in sign in the lift curve slope has been shown to be an indication of susceptibility to AWS.^{8, 11-16}

It should be noted that the flaps 10/10/5 configuration only represents one point in the sky at a particular moment in time in the scheduling of the control surfaces. The adverse conditions described above can normally be scheduled out by revision of the control laws. However, due to the rapidity and severity of an AWS event, this is not always obtainable.

The complexity of the flow field in the AWS region of interest is further illustrated in Figure 6, taken from reference 8, for the pre-production F/A-18E, flaps 10/10/5 at Mach 0.9 and 8 degrees AoA using *WIND* with the SST turbulence model. As illustrated in the figure, the flow is quite complex, involving

numerous vortices produced by the deflected control surfaces, several merging oblique and normal shock waves, and the presence of a large region of shock-induced separated flow. This type of flow is clearly beyond the scope of anything less than a RANS analysis to accurately capture all of the physics involved and to correctly compute the break in the lift curve. A comparison in the lift curves computed using *WIND* with experimental data obtained in the NASA Langley 16-ft transonic tunnel (16-ft TT)¹⁶ is presented in Figure 7 for both 0.8 and 0.9 Mach. The CFD results slightly under-predict the experimental lift at 0.8 Mach but the break in the lift curve slope is accurately predicted, while at 0.9 Mach, better agreement with the overall lift is achieved, but the break is predicted early. Very severe model dynamics were observed in the tunnel¹⁵ at 0.9 Mach in the region of the lift curve break and led to the decision to conduct time-accurate CFD calculations, which are discussed later.

Validation of Steady State CFD for AWS

Table 1 presents a sample of the configurations where RANS CFD solutions were obtained during the course of the AWS CFD investigation. It is by no means an exhaustive list, merely a representation of the level of effort that was expended in order to meet the goals set forth at the beginning of the program. In fact, the total number of solutions listed in the table represents about one-half of those generated. Also shown in the table are the aircraft configuration, the computer and number of processors that were used, grid sizes, and the memory requirements and CPU hours per solution. In general, the unstructured codes were much more memory intensive than the structured chimera code, however, *WIND* took approximately twice as long per processor to converge. But, since each of the codes used in this study achieve supra-linear speed-up with increasing number of processors (up to a point), the only limiting factor was the availability of the number of CPUs to perform the runs (memory is not a problem on massively parallel machines). So, with the grids developed, a solution for a particular Mach/AoA combination was usually produced within two to three days.

Very good qualitative agreement between the steady state RANS CFD with experimental oil flows was achieved as illustrated in Figures 8 and 9 for the F/A-18C, flaps 6/8/0 and the pre-production F/A-18E, flaps 10/10/5, respectively. In Figure 8 it can clearly be seen between the CFD solution and the oil flow results that the upper surface flow separated at the LE flap hinge line nearly all along the wingspan. Also

note that the influence of the LEX vortex on the wing flow is evident in both methods. Figure 9 presents a comparison near the break in the lift curve slope for the pre-production F/A-18E as shown in the RHS of Figure 7. Both the CFD result and the oil flow indicate that the separation has reached the LE flap hinge line in the region of the wing snag and here also, excellent correlation is achieved between the two methods when comparing the LEX influence on the wing flow and the attached flow near the wing tip. Figure 10 presents results prior to the break in the lift curve slope. Included in Figure 10 are results from a pressure sensitive paint test in the NASA Langley 16-ft TT.¹⁶ Each method shows a nearly full-span flow separation just forward of the TE flap hinge line. Careful examination of each result shows the influence of the wing snag on the separation pattern with a more forward separated region mid-span. It was determined that AWS on the pre-production F/A-18E was caused by a rapid popping of the flow separation reaching the LE flap hinge line in the vicinity of the snag over a very narrow AoA range (for certain Mach numbers, as little as 0.5 degrees).^{8, 13, 15, 16} If this rapid forward movement of separation occurs asymmetrically, wing drop could result.

Excellent quantitative agreement for the lift curve of the F-16N, flaps 0/0 at 0.8 Mach with experimental data was achieved using the *USM3D* code utilizing the SA turbulence model by Parikh and Chung¹³ as shown in Figure 11a. As the F-16N increases AoA, its maximum wing loading moves inboard¹³ in a smooth and continuous manner and is therefore not susceptible to AWS. In fact, it produces a nearly linear lift curve slope all the way up to 16 degrees AoA. Contrast that with the lift curves for the pre-production F/A-18E at both 0.8 and 0.9 Mach, shown in Figures 11b and 11c, respectively. Here, in the AWS region of interest (between 8 to 12 degrees AoA) the computational results either under-predict the lift or over-predict the lift and miss the experimental break in the lift curve slope.

Similar results were obtained for the AV-8B as shown in Figure 12 for both 0.3 and 0.75 Mach. In the AWS region of interest the *USM3D* solutions with the SA turbulence model tend to under-predict the lift and compute the break in the lift curve earlier than the experimental data. There were, however, some significant differences between the wind tunnel model and the CFD grid¹⁴ that may account for some of the discrepancy.

Quantitative comparison of the upper surface pressure coefficient distribution for the pre-

production F/A-18E, flaps 10/10/5, between a steady state *WIND* calculation and the experimental data is presented in Figure 13 at 0.9 Mach and 8 degrees AoA. As noted elsewhere,^{17,18} a feature of steady state RANS solutions is the sharpness of the shock wave prediction while the experimental result tends to be more smeared. If one compares Figure 13 with the RHS of Figure 7 it is apparent why the *WIND* results over-predict the lift coefficient at 8 degrees because the CFD shock locations are father aft than the experimental data, especially in the mid-span region of the wing. However, as noted earlier and in reference 15, large model dynamics were present for these conditions (suggesting an unsteady flow) and the experimental results represent an average of a moving shock, especially in the region of the wing LE snag. Therefore, a decision was made to perform time-accurate CFD calculations to determine if the agreement with the experimental data could be improved.¹⁸

Validation of Unsteady CFD for AWS

As noted by Schuster and Byrd,¹⁵ the pre-production F/A-18E with flaps 10/10/5 underwent severe pitch oscillations in the region of the break in the lift curve for 0.9 Mach. This dynamic behavior was traced to a rapid, aperiodic shock wave movement in the vicinity of the wing LE snag. The shock location would vary between a seemingly preferred bi-modal and even tri-modal state for a particular AoA. This suggested an inherently unsteady flow field and an *unstable* aerodynamic flow in terms of flow topology. At certain combinations of Mach/AoA, the shock location would remain somewhat steady for a given amount of time and then suddenly bounce to another location. The range of shock motion could be quite large (up to 27% chord) as it suddenly transitions from one dominant location to another less dominant location (and sometimes a third).

An initial attempt to try to model this behavior with time-accurate RANS calculations proved unsuccessful as shown in Figure 14. The LHS of the figure shows time-accurate upper surface pressure coefficient distributions for the pre-production F/A-18E, flaps 10/10/5 along a span-wise row just inboard of the LE snag. The calculations were performed using the *Cobalt* solver with the SA turbulence model at 0.9 Mach and 9.5 degrees AoA. The signals are rock-solid steady the entire time of the simulation. Contrast those results with the time-accurate calculations obtained using the DES¹⁹ turbulence option of *Cobalt* shown on the RHS of Figure 14. Now the unsteady nature of the flow is obvious (the

first two steady taps are on the LE flap which remains attached for this condition).

A comparison of the wing upper surface pressure coefficient distributions between the two approaches for the pre-production F/A-18E, flaps 10/10/5 is presented in Figure 15 for 0.9 Mach and 7 degrees AoA at a particular instant in time. The SA solution represents essentially a steady state solution while the DES results are presented at the instant in time when the flow separation is farthest forward. Quite significant chord-wise shock motion is apparent, with the subsequent differences in flow topology. This result provided confidence to perform a full range of (expensive) AoA calculations at 0.9 Mach to compare with the experimental data. Forsythe and Woodson present the results in reference 18 and the lift curve comparison for the pre-production F/A-18E for flaps 10/10/5 shown in Figure 16 is borrowed from their paper. Note that the RANS solutions either under- or over-predict the lift (and thus, shock location) and that the DES results are in much closer agreement with the experimental data. Also included in Figure 16 is a DES solution with grid adaptation,¹⁸ that correctly predicts the break in the lift curve and shows excellent agreement with the wind tunnel data. Thus, time-accurate CFD calculations can accurately model the unsteady flow in the AWS region of interest if one has the time and resources to perform the calculations. A recommended computational approach for the limited application of unsteady calculations in an overall steady RANS analysis for identifying AWS is provided in references 17 and 18.

F/A-18 C to E Wing Morphing Study

As mentioned earlier, one of the goals in the understanding of AWS was to try to determine why the pre-production F/A-18E was susceptible to AWS while the F/A-18C from which it was derived, is not. The two most significant geometric contributors to AWS on the pre-production F/A-18E, as reported by Green and Ott,¹² were found to be the addition of the wing LE snag and the reduction in LE flap chord ratio. Figure 17 shows a comparison of the upper surface flow separation patterns between the baseline F/A-18C and a “morphed” F/A-18C with the addition of a wing LE snag and the same LE flap chord taper ratio as that which was incorporated on the F/A-18E.

The comparisons were performed at 0.9 Mach for various AoA with the flaps set at 6/8/0. Here higher speed flow is shown as blue/purple and lower speed flow is indicated by green/yellow. The flow over the baseline F/A-18C remains attached up until the TE flap hinge line for each of the AoA shown, while for

the morphed configuration, even at 7 degrees, the influence of the LE snag is apparent with the separation moving forward in the snag region. As AoA further increases, the separation continues forward until at 9 degrees, it has reached the LE flap hinge line in the snag region, producing a significant loss in lift and a change in sign of the slope in the wing root bending moment coefficient, as noted. Changes in sign of the slope of the wing root-bending moment coefficient is an indication of potential lateral problems.¹¹⁻¹⁴ A thorough description of the morphing study is provided in reference 12.

Concluding Remarks

Several CFD methods have been successfully applied to provide a better understanding of the underlying physics contributing to AWS. It was determined that AWS is caused by a large transition of flow separation moving from the trailing edge to the LE flap hinge line on the upper surface of a wing undergoing transonic maneuvers. If it occurs asymmetrically, large rolling moments are produced and flight safety could be put at risk.

Although useful information may be gained from lower order methods, at least a steady state RANS analysis is required for a thorough understanding of the aerodynamic phenomena causing AWS. The severity of dynamic AWS events was accurately modeled using time-accurate CFD with a hybrid RANS/LES computational approach.

Acknowledgements

The authors wish to express their gratitude to the Office of Naval Research and Mr. Lawrence Ash for sponsoring this research. We are indebted to Dr. Bill Strang and Mr. Ken Wurtzler of Cobalt Solutions, for their expert assistance. Special thanks are due to Mr. Joe Chambers of Ball Aerospace and Mr. Joe Laiosa from NAVAIR for their continued guidance and support throughout this endeavor. We would also like to thank each of the other members of the AWS Program team, particularly Dr. Bob Hall, for their constructive criticism and helpful suggestions, which have proven to be invaluable. The first author sincerely appreciates the contribution of Dr. Chris Bruner of Hewlett-Packard – a real airplane guy – for his excellent insights. Lastly, the computational resources provided by the DoD High Performance Computing Modernization Office (HPCMO) is gratefully acknowledged, without which, none of this work would have been possible.

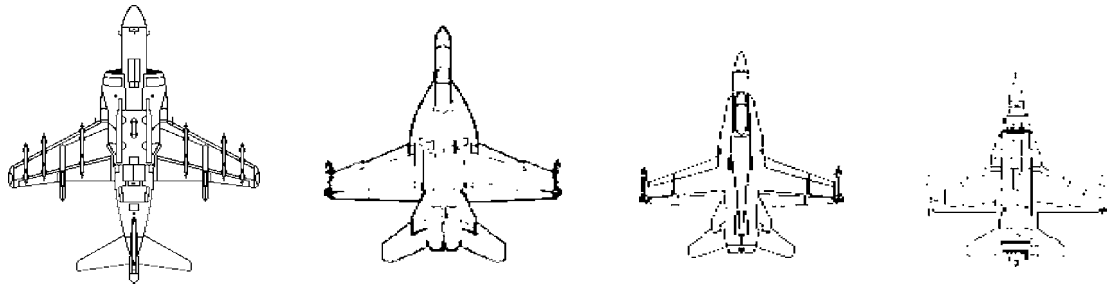
References

1. Hall, R.M., and Woodson, S.H.: "Introduction to the Abrupt Wing Stall Program," AIAA-03-0589, January 2003.
2. Chambers, J., and Hall, R.M.: "Historical Review of Uncommanded Lateral-Directional Motions at Transonic Conditions (Invited)," AIAA-03-0590, January 2003.
3. Frink, N.T.: "Tetrahedral Unstructured Navier-Stokes Method for Turbulent Flows", *AIAA Journal*, Vol. 36, No. 11, November 1998, pp. 1975-1982.
4. Spalart, P.R., and Allmaras, S.R.: "A One-Equation Turbulence Model for Aerodynamic Flows," *La Recherche Aerospatiale*, Vol. 1, 1994.
5. Bhat, M.K., and Parikh, P.C.: "Parallel Implementation of an Unstructured Grid-Based Navier-Stokes Solver," AIAA-99-0663, January 1999.
6. Bush, R.H., Tower, G.D., and Towne, C.E.: "*WIND*: The Production Flow Solver of the NPARC Alliance," AIAA-98-0935, January 1998.
7. Menter, F.R.: "Zonal Two Equation $k-\omega$ Turbulence Models for Aerodynamic Flows," AIAA-93-2906, January 1993.
8. Grove, D.V., Laiosa, J.P., Woodson, S.H., and Stookesberry, D.C.: "Computational Fluid Dynamics Study of an Abrupt Wing Stall Phenomena on the F/A-18E," AIAA-02-1025, January 2002.
9. Strang, W.Z., Tomaro, R.F., and Grismer, M.J.: "The Defining methods of *Cobalt₆₀*: A Parallel, Implicit, Unstructured Euler/Navier-Stokes Flow Solver," AIAA-99-0786, January 1999.
10. Gottlieb, J.J. and Groth, C.P.T.: "Assessment of Reimann Solvers for Unsteady One-Dimensional Inviscid Flows of Perfect Gases," *Journal of Computational Physics*, Vol. 78, pp. 437-458, 1988.
11. Lamar, J.L., and Hall, R.M.: "Abrupt Wing Stall Figure of Merit Developed Parameters from Static Transonic Model Tests," AIAA-03-0745, January 2003.
12. Green, B.E., and Ott, J.D.: "F/A-18C to E Wing Morphing Study for the Abrupt Wing Stall Program," AIAA-03-0925, January 2003.
13. Parikh, P.C., and Chung, J.J.: "A Computational Study of the Abrupt Wing Stall for Various Fighter Jets: Part I, F/A-18E and F-16N," AIAA-03-0746, January 2003.
14. Chung, J.J., and Parikh, P.C.: "A Computational Study of the Abrupt Wing Stall for Various

- Fighter Jets: Part II, AV-8B and F/A-18C,” AIAA-03-0747, January 2003.
15. Schuster, D., and Byrd, J.: “Transonic Unsteady Aerodynamics of the F/A-18E at Conditions Promoting Abrupt Wing Stall,” AIAA-03-0593, January 2003.
 16. McMillin, S.N., Hall, R.M., and Lamar, J.L.: “Transonic Experimental Observations of Abrupt Wing Stall on an F/A-18E Model,” AIAA-03-0591, January 2003.
 17. Woodson, S.H., Green, B.E., Chung, J.J., Grove, D.V., Parikh, P.C., and Forsythe, J.R.: “Recommendations for CFD Procedures for Predicting Abrupt Wing Stall,” AIAA-03-0923, January 2003.
 18. Forsythe, J.R., and Woodson, S.H.: “Unsteady CFD Calculations of Abrupt Wing Stall Using Detached-Eddy Simulation,” AIAA-03-0594, January 2003.
 19. Spalart, P.R., Jou, W.H., Strelets, M., and Allmaras, S.R.: “Comments on the Feasibility of LES for Wings and on a Hybrid RANS/LES Approach,” *Advances in DES/LES, 1st AFOSR Int. Conf. On DES/LES*, Aug. 4-8, 1997, Greyden Press, Columbus, OH.

Table 1. Sample of Aircraft Configurations and Computational Requirements for the AWS Study.

Aircraft Configuration	Code & Turbulence Model	Computer/Number of Processors	Memory Requirement	CPU Hours Per Case	Number of Cases Run	Grid Size
F/A-18C flaps 6/8/0 no LEX fence	<i>Cobalt</i> / SST	Linux Cluster/ 60	17GB	2880	M = 0.85/ 8 AoA	5.7M TETS
F/A-18C flaps 6/8/0 with LEX fence	<i>USM3D</i> /SA	SGI Origin 3000/ 30	9.5GB	2500	M = 0.85/ 11 AoA M = 0.9/ 9 AoA	6.8M TETS
F/A-18E flaps 10/10/5 No tails	<i>USM3D</i> / SA	SGI Origin 2000/ 40	5.42GB	1280	M = 0.8/ 6 AoA M = 0.9/ 7 AoA	3.8M TETS
F-16N flaps 0/0	<i>USM3D</i> / SA	SGI Origin 3000/ 48	9.98GB	2500	M = 0.8/ 6 AoA	6.9M TETS
AV-8B flaps 0/5,10,15,20	<i>USM3D</i> /SA	SGI Origin 3800/ 30	13GB	3000	M = 0.75/ 8 AoA M = 0.8/ 10 AoA M = 0.9/ 11 AoA	9M TETS
F/A-18C flaps 6/8/0 & 11 Morphed Configurations	<i>WIND</i> /SST	SGI Octane, Origin 2000 & Origin 3000/ 12 to 32	900MB	6000	M = 0.8, 0.9/ 6 AoA	13.9M POINTS
F/A-18E flaps 6/8/4 No tails	<i>WIND</i> /SST	SGI Power Challenge Array/ 12 to 32	1.2GB	6000	M = 0.9/ 6 AoA	13M POINTS
F/A-18E flaps 10/10/5 No tails	<i>WIND</i> /SST	SGI Power Challenge Array/ 12 to 32	1.2GB	6000	M = 0.9/ 6 AoA	13M POINTS
F/A-18E flaps 10/10/5 No tails	<i>Cobalt</i> /SA	IBM SP3/ 80	19GB	4000	M = 0.9/ 6 AoA	7.2M TETS/PRISMS
F/A-18E flaps 10/10/5 No tails	<i>Cobalt</i> /DES	Compaq ES45/ 64	24GB	9000	M = 0.9/ 6 AoA	9.2M TETS/PRISMS



	AV-8B	F/A-18E	F/A-18C	F-16N
Aspect ratio	4.0	3.5	3.5	3.2
Taper ratio	0.30	0.302	0.35	0.2275
Leading edge (LE) sweep angle	36	29.4	26.7	40.0
Maximum thickness	11.5	6.2	5.0	4.0
Twist	-8.0	0.0	0.0 to 145.39, 4.0 at 224.5	3.0
Dihedral	-11.0	-3.0	-3.0	0.0

Figure 1. Geometric properties of aircraft considered in the AWS study.

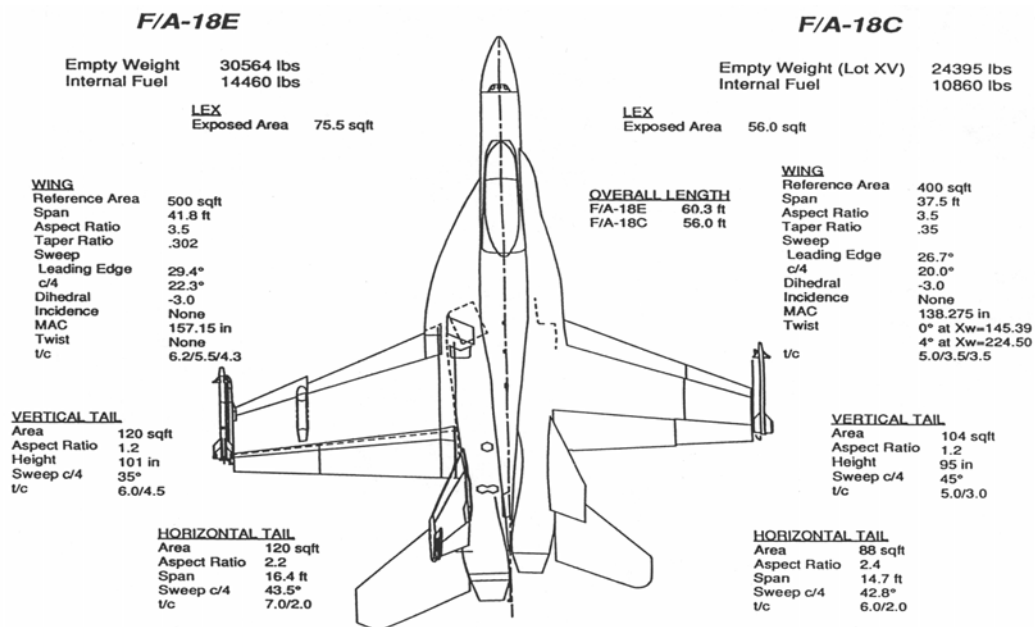


Figure 2. Wing parameter design differences between the F/A-18C and the F/A-18E aircraft.

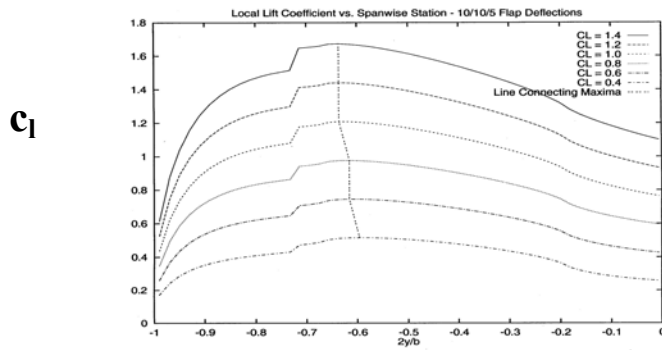


Figure 3a. Span-wise lift coefficient distribution for the pre-production F/A-18E, flaps 10/10/5 using a panel code.

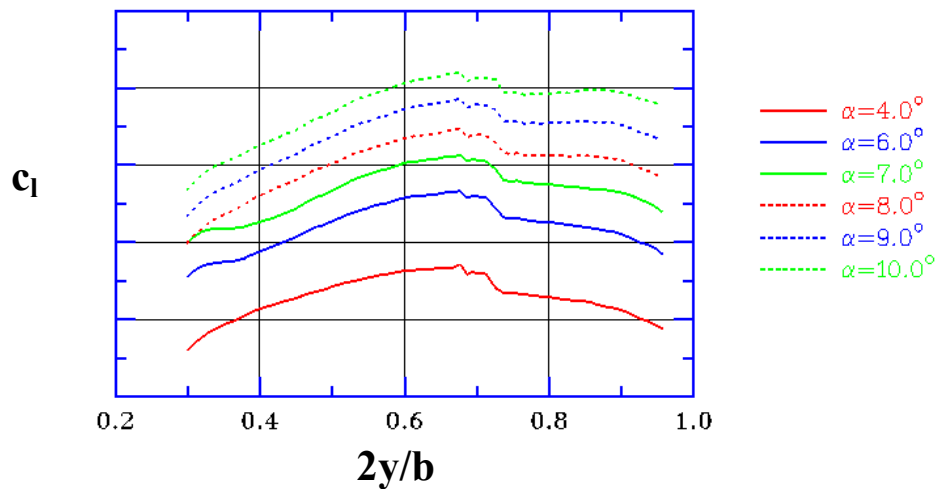


Figure 3b. Span-wise lift coefficient distribution for the pre-production F/A-18E, flaps 10/10/5 at 0.8 Mach using *USM3D* inviscid.

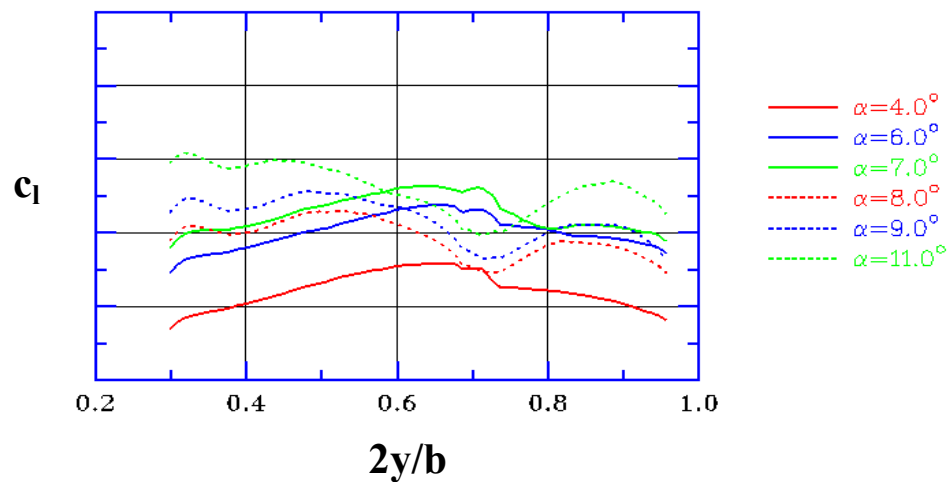


Figure 3c. Span-wise lift coefficient distribution for the pre-production F/A-18E, flaps 10/10/5 at 0.8 Mach using *USM3D/SA* viscous.

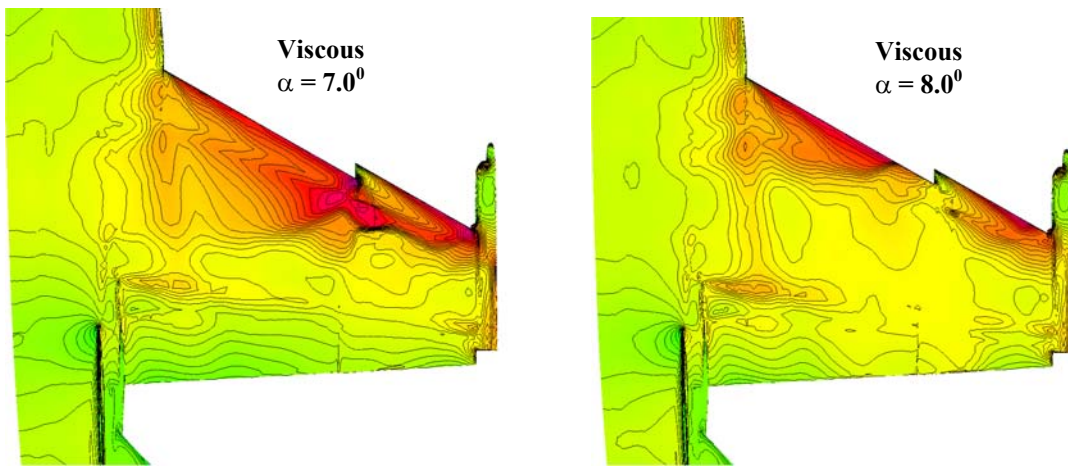


Figure 4. Comparison of the upper surface pressure coefficient distributions between 7 and 8 degrees AoA for the F/A-18E, flaps 10/10/5 using *USM3D/SA* viscous.

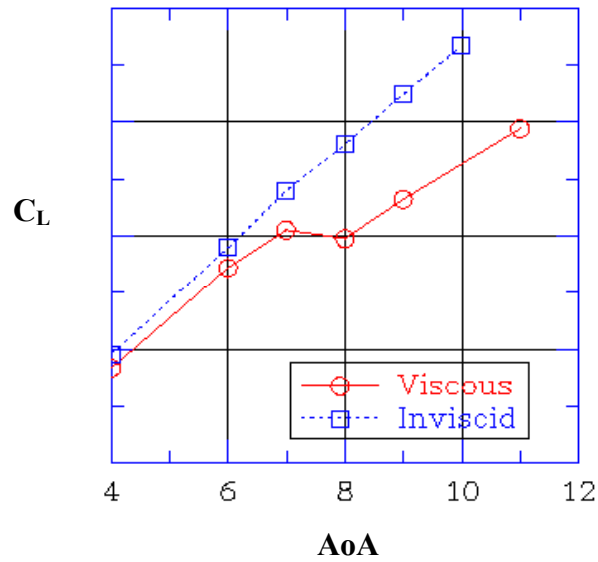


Figure 5. Comparison of the lift coefficient for the F/A-18E flaps 10/10/5 between the inviscid and viscous *USM3D* solutions.

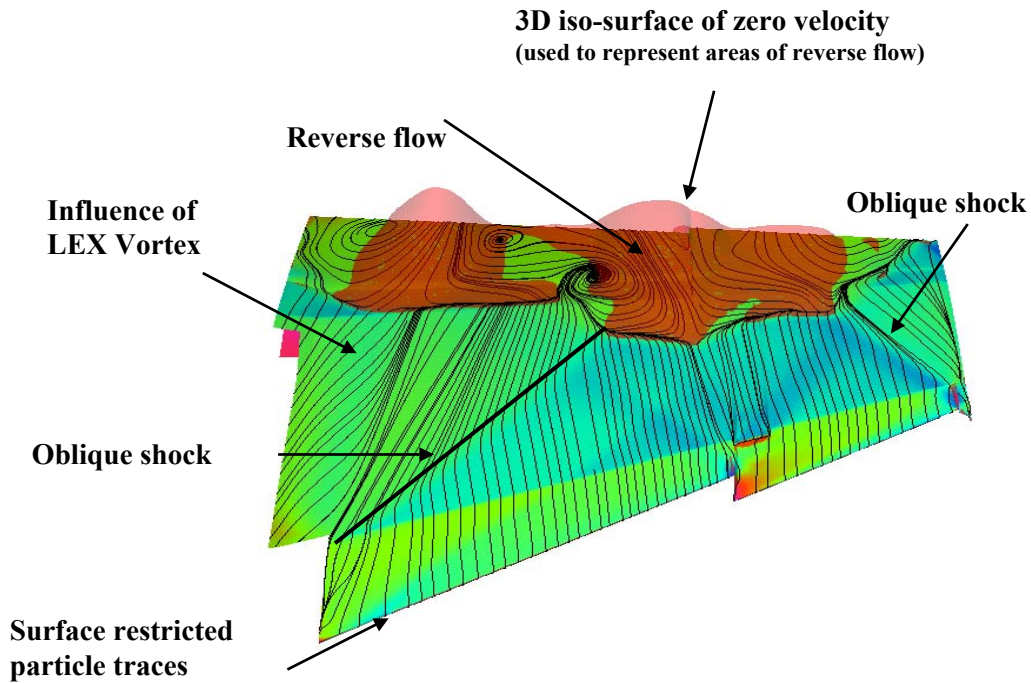


Figure 6. Wing upper surface flow over the F/A-18E flaps, 10/10/5 at 0.9 Mach and 8 degrees AoA computed using WIND/SST.

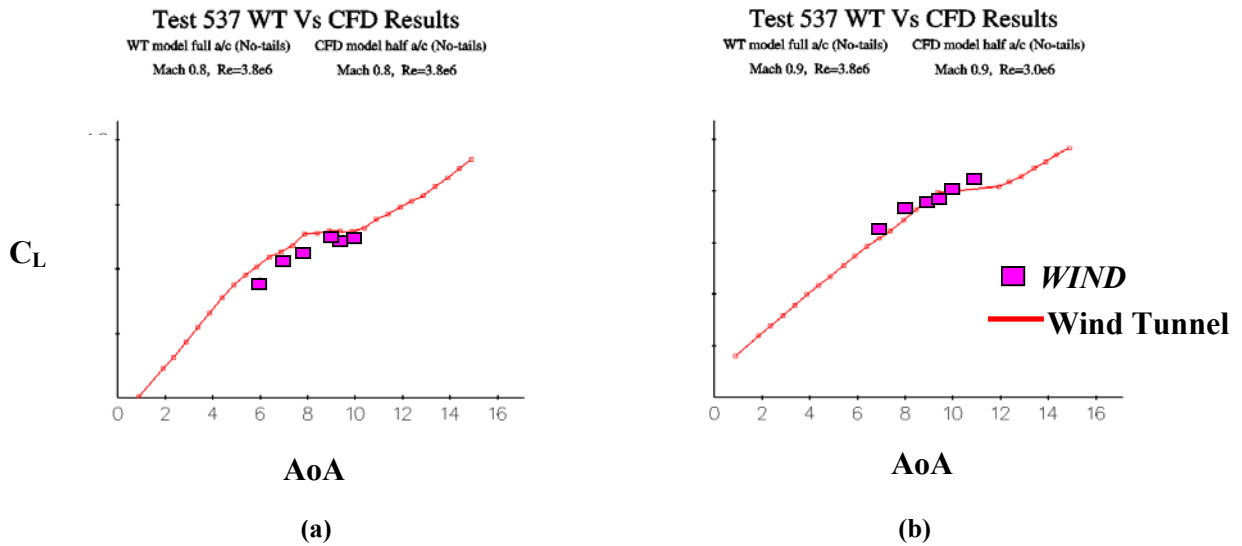


Figure 7. Comparison of the lift coefficient for the F/A-18E flaps, 10/10/5 between WIND/SST and wind tunnel results for: (a) 0.8 Mach and (b) 0.9 Mach.

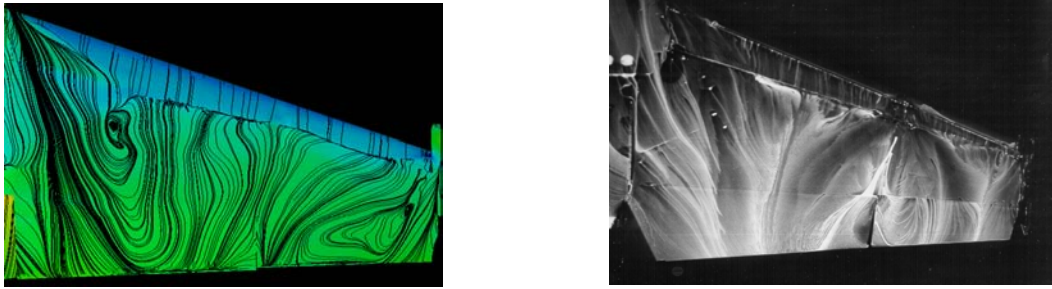


Figure 8. Comparison of CFD surface restricted particle traces with wind tunnel oil flow for the F/A-18C, flaps 6/8/0 at 0.85 Mach and 10 degrees AoA using *Cobalt/SA*.

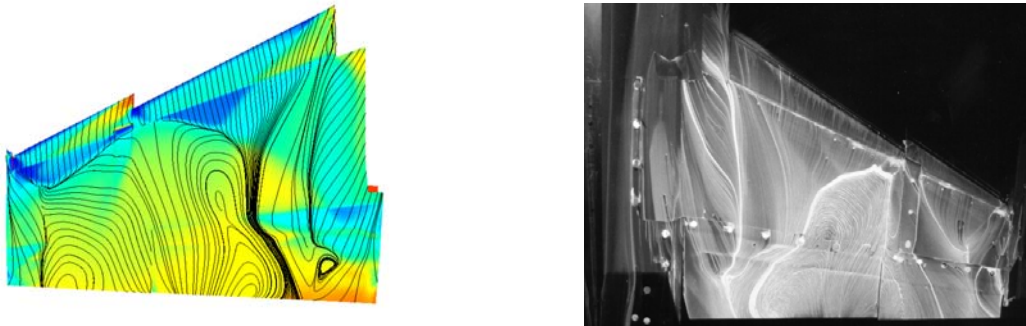


Figure 9. Comparison of CFD surface restricted particle traces with wind tunnel oil flow for the F/A-18E, flaps 10/10/5 at 0.9 Mach and 10 degrees AoA using *WIND/SST*.



Figure 10. Comparison of CFD surface restricted particle traces with oil flow and pressure sensitive paint for the F/A-18E, flaps 10/10/5 at 0.9 Mach and 8 degrees AoA using *WIND/SST*.

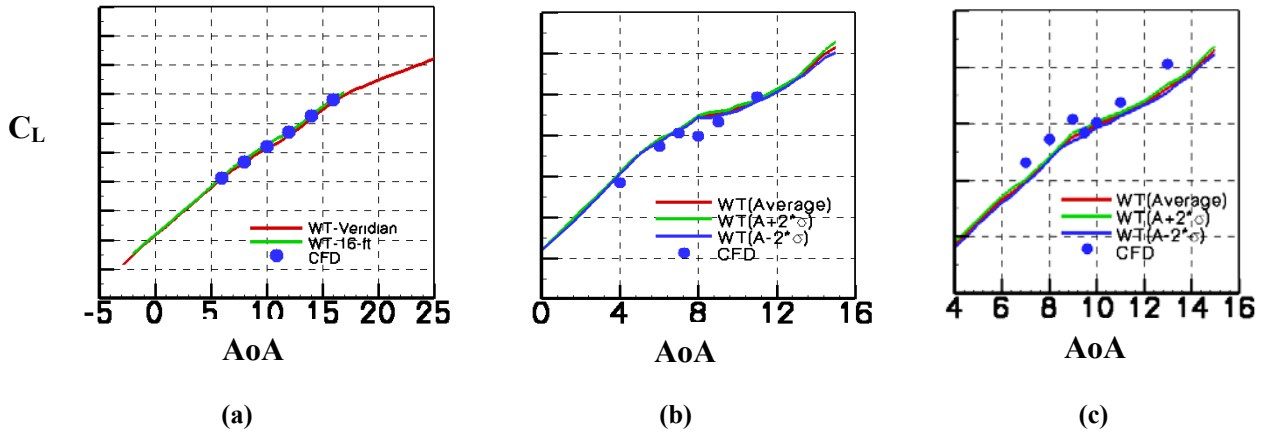


Figure 11. Lift coefficient comparisons between *USM3D* /SA and experimental data for: (a) F-16N, flaps 0/0 at 0.9 Mach, (b) F/A-18E, flaps 10/10/5 at 0.8 Mach, and (c) F/A-18E, flaps 10/10/5 at 0.9 Mach.

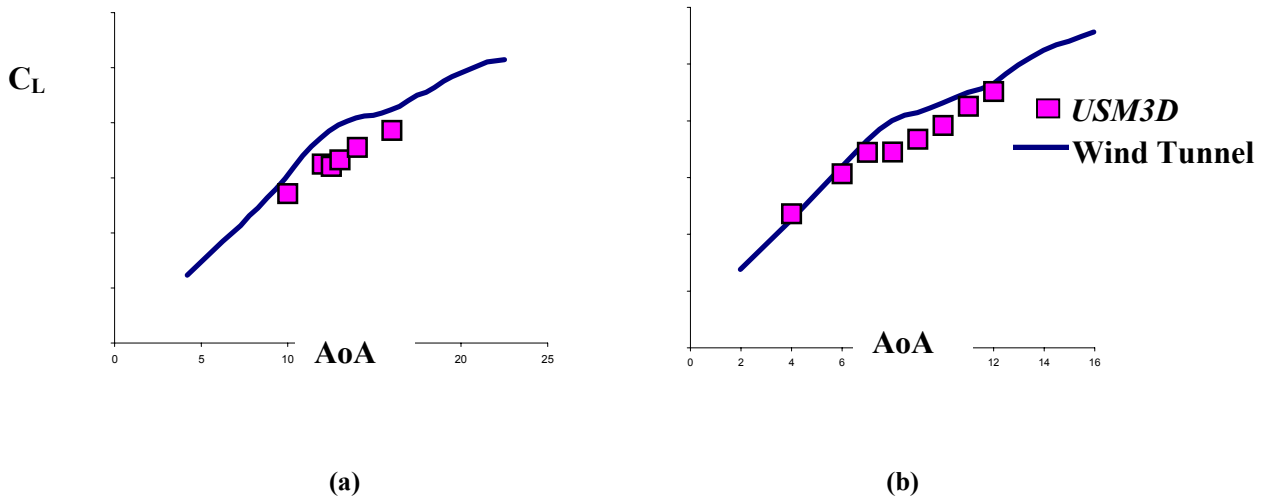


Figure 12. Lift coefficient comparisons between *USM3D*/SA and experimental data for: (a) AV-8B, flaps 0/25 at 0.3 Mach, and (b) AV-8B, flaps 0/10 at 0.75 Mach.

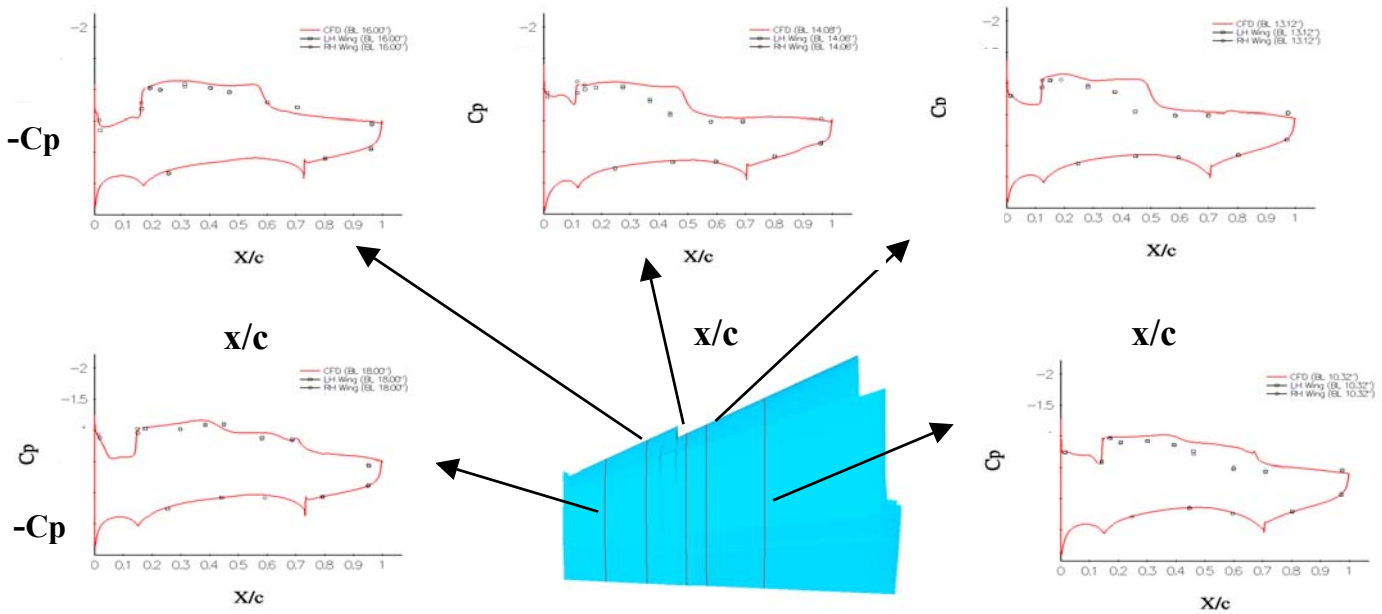


Figure 13. Comparison of upper surface pressure coefficient distributions for the F/A-18E, $x/c = 10/5$ at 0.9 Mach and 8 degrees AoA using *WIND/SST*.

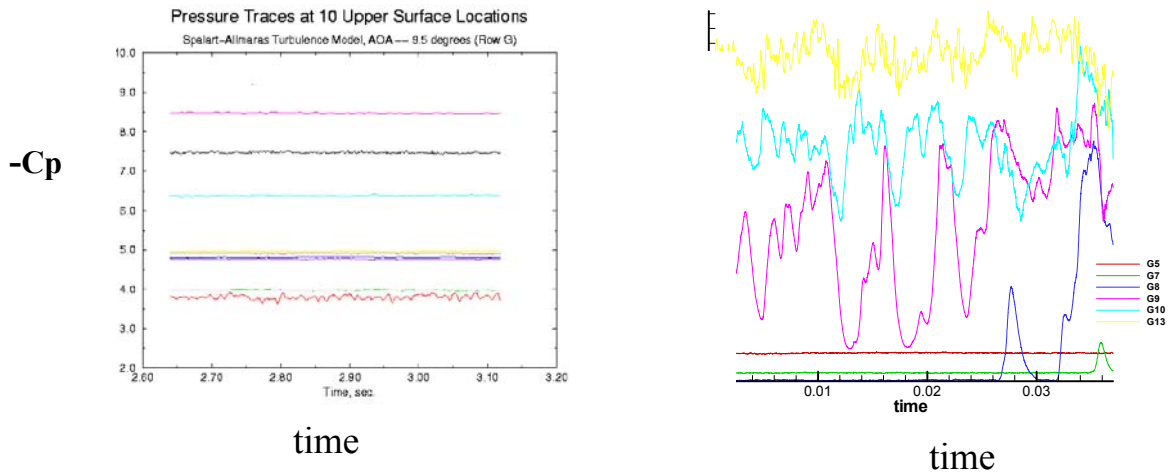


Figure 14. Comparison of upper surface pressure coefficient signals near mid-span for the F/A-18E, flaps 10/10/5 at 0.9 Mach and 9.5 degrees AoA using the *Cobalt SA* and *DES* turbulence models.

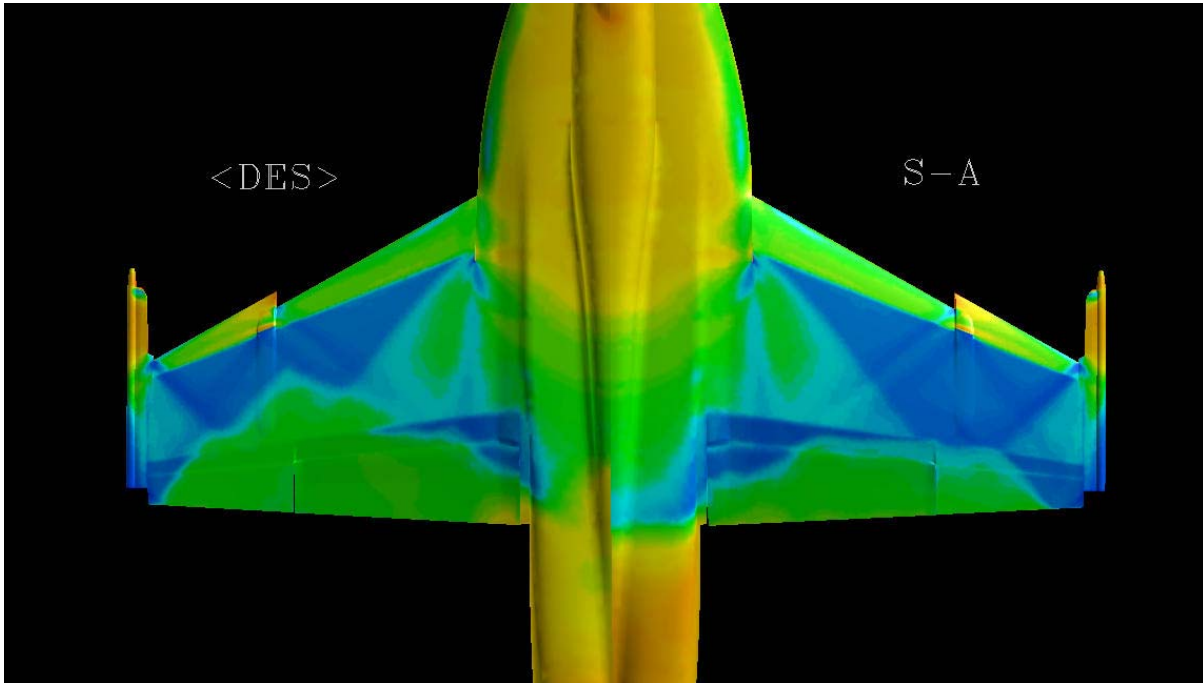


Figure 15. Comparison of upper surface pressure coefficient distributions for the F/A-18, flaps 10/10/5 at 0.9 Mach and 7 degrees AoA using the time-accurate *Cobalt* DES and SA turbulence models.

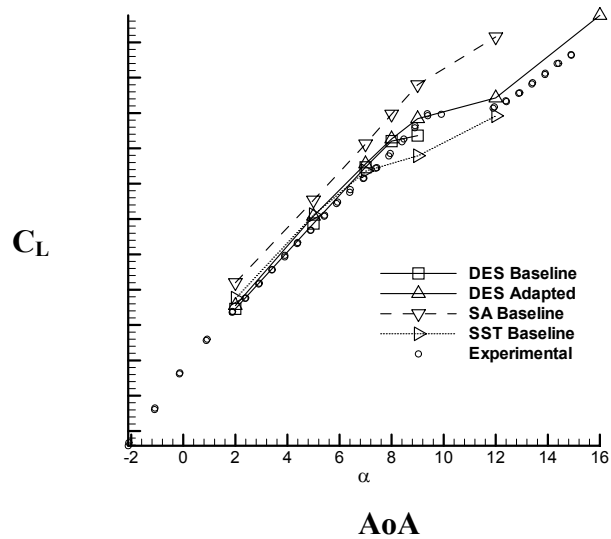
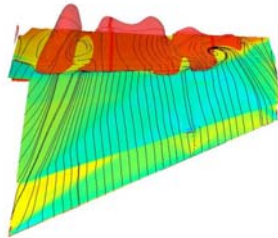
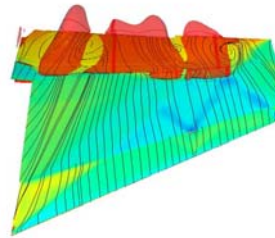


Figure 16. Steady state vs. time-averaged lift coefficient for the F/A-18E, flaps 10/10/5 at 0.9 Mach using the *Cobalt* DES, SA, and SST turbulence models with the experimental data.

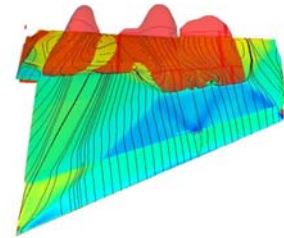
F/A-18C



7 Degrees

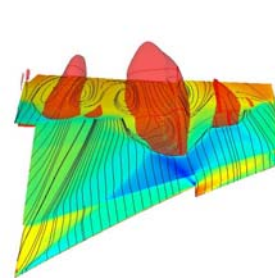
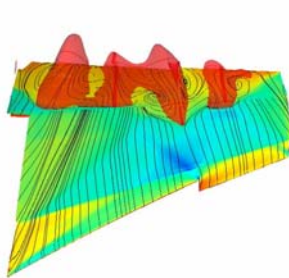


8 Degrees



9 Degrees

F/A-18C with a LE Snag & Tapered LE Flap



Slope of WRBM changes
sign at 8 degrees

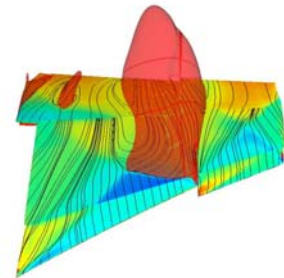


Figure 17. Upper surface flow separation patterns for the F/A-18C and the F/A-18C with a LE snag and reduced LE flap chord ratio, both with flaps 6/8/0 using *WIND/SST*.